International Journal of Engineering Trends and Technology
ISSN: 2231–5381 / https://doi.org/10.14445/22315381/IJETT-V72I11P114

Volume 72 Issue 11, 106-116, November 2024

Original Article

A New Mixed Ligand Copper (II) Complex: Synthesis, Crystal Structure and Hirshfeld Surface Analysis

Toshtemirov A. E[1], Turaev Kh. Kh[2], Ibragimov A. B[3], Umbarov I. A[4], Ashurov J. M[5], Alimnazarov B. Kh[6]

[1,2,4,6]*Faculty of Chemistry, Termez State University, Termez, Uzbekistan.*
[3]*Institute of General and Inorganic Chemistry, Academy of Sciences of Uzbekistan, Tashkent, Uzbekistan.*
[5]*Institute of Bioorganic Chemistry, Academy of Sciences of Uzbekistan, Tashkent, Uzbekistan.*

[1]*Corresponding Author : tosabdurasul20@gmail.com*

Received: 29 May 2024 Revised: 07 October 2024 Accepted: 15 October 2024 Published: 29 November 2024

Abstract *- In this article, the optimal conditions for synthesizing a new [Cu(phen)(HSO$_4$)$_2$•2H$_2$O] metal complex with the ligand 1,10-phenanthroline and the metal ion Cu (II) were investigated. The obtained complex was analyzed using various physicochemical methods such as X-ray diffraction analysis for determining the molecular structure of the single crystal, elemental analysis, IR spectra, UV-vis, DTA, and TGA. The complex crystallized in a monoclinic form with the P21/n space group. According to the XRD results of the single crystal investigation, it was determined that the Cu (II) complex cation exhibits distorted square-pyramidal geometry with the Jahn-Teller effect in the CuN$_2$O$_4$ core. Additionally, the Hirshfeld surface analysis was studied.*

Keywords *- Crystal, X-ray, 1,10-fenantrolin, Hirshfeld surface, IR-spectra, UV-vis.*

1. Introduction

The synthesis of new compounds and functional materials is advancing in the field of inorganic chemistry. Various methodologies have been employed for this purpose. Many transition metal complexes are synthesized due to their structural diversity and biological importance [1,2]. In particular, copper (II) ions, the third most abundant transition metal in humans, are essential for many organisms. This metal is required for aerobic metabolism and can be found as an active site or a structural component of a large number of enzymes [3-5]. The antibacterial properties of metal complexes containing 1,10-phenanthroline [6], as well as the synthesis, crystal structures, and magnetic properties of metal complexes of 1,10-phenanthroline and sulfonate groups, have been studied [7]. Several complexes of 1,10-phenanthroline with copper metal, such as Cu(fen)3(S8), Cu(phen)3, [Cu(phen)2(OS2O7)], and Cu(phen)2(FBF3), have been synthesized. The crystal structures of these compounds have been determined using X-ray crystallographic methods [8,9]. Two new organic-inorganic hybrid supramolecular compounds based on 1,10-phenanthroline, [Zn(phen)(SO_4)(H_2O)$_2$]n and [Cu(phen)(H_2O)$_2$]SO_4, have also been synthesized. Their physicochemical properties have been studied and analyzed using IR spectroscopy, Thermogravimetric Analysis (TGA), and luminescence spectroscopy [8]. 1,10-phenanthroline is a heterocyclic compound that is one of the most popular bidentate N, N-chelating agents used in coordination chemistry. Metal complexes formed by 1,10-phenanthroline with metal cations have photochemical and photophysical properties. 1,10-phenanthroline is biologically active, so it is interesting to study the biological effects of its complexes [10]. This study aims to synthesize a new complex compound based on Cu^{2+} and 1,10-phenanthroline and to investigate the composition, structure, and physicochemical properties of the obtained complex compounds.

2. Experimental Part

2.1. Methods

In this study, the composition, structure, and other properties of the synthesized complex were determined using X-ray Structure Analysis (XRD), IR spectroscopy, Thermal Analysis (TGA, DTA), UV, and elemental analysis methods.

2.2. Materials and Methods

All the chemicals used were obtained from Sigma-Aldrich and used as received. The elemental percent composition of compounds was determined by the Dumas method using ELEMENTARY UNICUBE® IZI equipment (C, H, O, N, S). The FT-IR spectra of the coordination compounds were recorded in the solid state in the range from 4000 cm-1 to 400 cm-1 with 16 scans and a spectral resolution of 4 cm-1 on an IR-Fourier spectrometer IRTracer-100 (Shimadzu, Japan) calibrated with KBr (Detector setting: RT-DLaTGS). The DTG-60 Simultaneous DTA-TG apparatus from Shimadzu was used to obtain results from Thermogravimetric (TG) and Differential Thermal Analysis (DTA). The tested sample was initially held at 30 ◦C in an

argon atmosphere with a flow rate of 100 ml/min for 10 min, followed by heating at a rate of 10 ◦C/min. The UV-vis spectrophotometer EMC-30PC-UV (EMC Labs Germany) was used to record the absorption spectra of the sensors.

2.3. X-Ray Crystallography

Reflection sets were obtained at 293 K using an XtaLAB Synergy HyPix3000 diffractometer (micro-focus sealed X-ray tube with Cu-anode (λ=1.54184 Å)). Experimental data were collected using the CrysAlisPro program [11]. An absorption correction was applied using the multi-scan method within the same program. The structures were solved using the direct method with the SHELXT program package [12, 13] and refined using full-matrix least squares with the SHELXL program [12].

Molecular drawings were generated using the MERCURY program package [14, 15]. Crystallographic data have been deposited with the Cambridge Crystallographic Data Centre under deposit number 2349812. Check CIF/Platon reports for these structures, which are provided in the supplementary material. Crystal data and experimental details for the complex compound are summarized in Table 1. Selected bond distances and angles are listed in Table 2.

2.4. Hirshfeld Surface Calculations

CrystalExplorer21.5 [16] was used to carry out the Hirshfeld Surface (HS) analysis and the associated 2D fingerprinting. For the title compounds, the HS was mapped using a dnorm and shape index ranging from -0.5 to 1.0 Å for the dnorm and -1.0 to 1.0 Å for the shape index.

2.5. Synthesis, Element Analysis

All substances were weighed on an analytical balance. $CuSO4•5H_2O$ (0.5 g, 2 mmol) and 1,10-phenanthroline (0.36 g, 2 mmol) were used. Then, 0.05 molar solutions of all substances were prepared. The metal salt was dissolved in water, and 1,10-phenanthroline was dissolved in ethanol. The solutions were mixed, and 40 ml of 0.05 molar sulfuric acid solution was added to the resulting mixture. It was then vigorously stirred at 70°C for 25 minutes using a magnetic stirrer. The resulting solution was left in an open beaker at room temperature.

After 3 days, blue monocrystals were observed at the bottom of the glass (Figure 2). Crystals suitable for X-ray diffraction analysis were separated under a microscope and washed with ethanol. Subsequently, crystals suitable for X-ray diffraction analysis were separated and examined, revealing the formation of a $[Cu(phen)(HSO_4)_2•2H_2O]$ complex. The elemental percent composition of the compound was determined by the Dumas method on ELEMENTARY UNICUBE® IZI equipment. For compounds with a composition of $C_{12}H_{14}CuN_2O_{10}S_2$ calculated C, 30.41; H, 2.98; N, 5.91; O, 33.76; S, 13.53 %, found C, 30.40; H, 2.97; N, 5.89; O, 33.68; S, 13.38%.

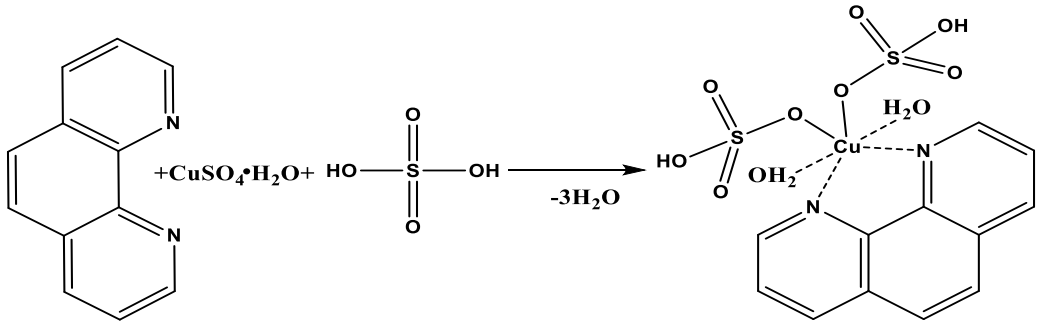

Fig. 1 The synthesis reaction of the complex $[Cu(phen)(HSO_4)_2•2H_2O]$

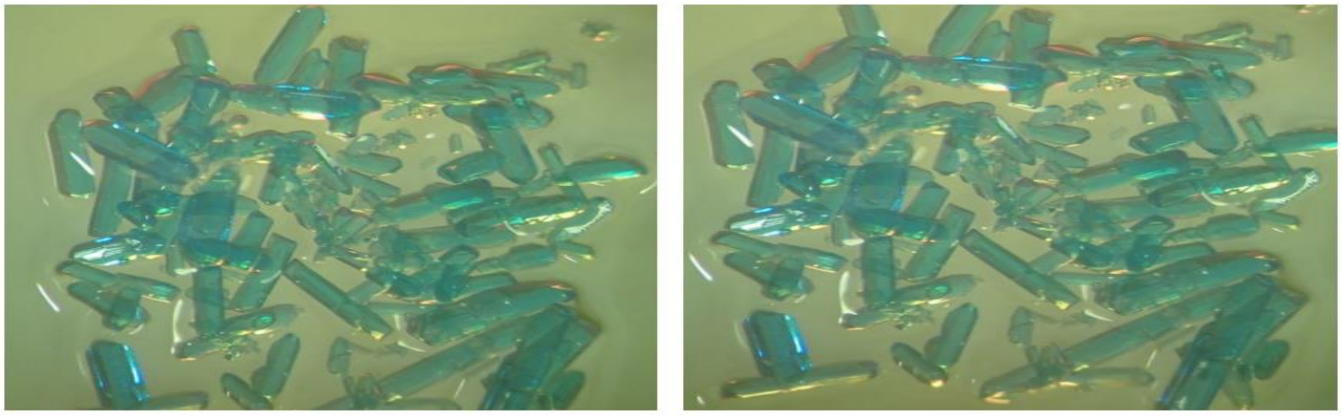

Fig. 2 Blue monocrystals in a glass beaker were captured using an Infinix HOT 40 phone camera under the MBS-9 microscope

Table 1. Crystal data and structure refinement parameters

Crystal data	
$C_{12}H_{14}CuN_2O_{10}S_2$	Z = 7
M_r = 475.95	F(000) = 1697.833
Monoclinic, $P2_1/n$	D_x = 3.319 Mg m^{-3}
a = 7.2944 (2) Å	Cu Ka radiation, l = 1.54184 Å
b = 11.2466 (3) Å	Cell parameters from 1831 reflections
c = 20.5213 (7) Å	q = 4.0-61.5°
b = 98.073 (3)°	m = 8.35 mm^{-1}
V = 1666.83 (9) Å^3	
Data collection	
Xcalibur, Ruby diffractometer	2054 reflections with I i 2u(I)
Detector resolution: 10.2576 pixels mm^{-1}	R_{int} = 0.038
w scans	q_{max} = 61.9°, q_{min} = 4.4°
Absorption correction: multi-scan *CrysAlis PRO* 1.171.38.41 (Rigaku Oxford Diffraction, 2015) Empirical absorption correction using spherical harmonics, implemented in SCALE3 ABSPACK scaling algorithm.	h = -8®4
T_{min} = 0.569, T_{max} = 1.000	k = -12®10
4796 measured reflections	l = -22®23
2557 independent reflections	
Refinement	
Refinement on F^2	0 restraints
Least-squares matrix: full	26 constraints
$R[F^2 > 2s(F^2)]$ = 0.048	H-atom parameters constrained
$wR(F^2)$ = 0.130	$w = 1/[s^2(F_o^2) + (0.0615P)^2 + 1.2868P]$ where $P = (F_o^2 + 2F_c^2)/3$
S = 1.09	$(D/s)_{max}$ = 0.0003
2557 reflections	$D\rho_{max}$ = 0.67 e Å^{-3}
249 parameters	$D\rho_{min}$ = -0.54 e Å^{-3}

Table 2. Selected bond lengths (Å) and angles (°) for complex compound

Cu1—O9	2.472 (3)	O2—Cu1—O9	86.10 (12)
Cu1—O2	2.002 (3)	O1—Cu1—O9	84.17 (13)
Cu1—O1	1.981 (3)	O1—Cu1—O2	93.60 (13)
Cu1—N2	2.008 (4)	N2—Cu1—O9	89.48 (14)
Cu1—O3	2.339 (4)	N2—Cu1—O2	173.38 (14)
Cu1—N1	2.003 (4)	N2—Cu1—O1	90.84 (14)
S2—O7	1.457 (3)	O3—Cu1—O9	173.78 (13)
S2—O9	1.443 (3)	O3—Cu1—O2	90.65 (15)
S2—O10	1.564 (3)	O3—Cu1—O1	90.75 (15)
S2—O8	1.442 (3)	O3—Cu1—N2	94.20 (16)
S1—O6	1.475 (4)	N1—Cu1—O9	96.91 (13)
S1—O4	1.458 (3)	N1—Cu1—O2	93.18 (14)
S1—O3	1.412 (4)	N1—Cu1—O1	173.18 (14)
S1—O5	1.542 (4)	N1—Cu1—N2	82.45 (15)
		N1—Cu1—O3	88.55 (15)

3. Results and Discussion

3.1. The X-Ray Structure of the Complex

The molecular structure of the complex is shown in Figure 3. The packing diagram is shown in Figure 4. The selected bond lengths and angles are presented in Table 2. The Cu (II) ion is coordinated with two nitrogen atoms (N1, N2) of the 1,10-phenanthroline ligand, two oxygen atoms (O1, O2) from water molecules, and two oxygen atoms (O3, O9) from the sulfate. In the complex, the O1, O2, N1, and N2 atoms form equatorial coordination around the Cu (II) ion, while the O3 and O9 atoms occupy axial positions.

The average Cu-O1, Cu-O2, Cu-O3, and Cu-O9 distances are 1.981(3), 2.002(3), 2.339(4), and 2.472(4) Å, respectively. The Cu-N1 and Cu-N2 distances are longer at 2.003(4) and 2.008(3) Å, respectively. The bond angle O3-Cu1-O9 deviates slightly from the ideal value of 180°, measuring 178.72°. Calculating the bond lengths and angles around the central metal ion reveals that the Cu cation is located in a distorted octahedral environment. The crystallization of the complex involves intermolecular H-bonding and π-π stacking interactions, as depicted in Figure 5. Therefore, the interplay between H-bonding and π-π stacking interactions plays an important role in the stability of the crystal lattice.

3.2. IR Spectrum Analysis of Co (II) Complex

The FT-IR spectrum of the coordination compound was recorded in the solid state in the range from 4000 cm^{-1} to 600 cm^{-1} with 20 scans and a spectral resolution of 4 cm^{-1}. The FT-IR spectrum of 1,10-phenanthroline is shown in Figure 3. The FT-IR spectrum of the ligand 1,10-phenanthroline includes four main characteristic vibrational bands: the stretching vibration bands of the C=N and C=C double bonds appear at 1616 cm^{-1} and 1587 cm^{-1} for 1,10-phenanthroline, respectively. The absorption bands corresponding to the vibrations occurring in the ring plane of the 1,10-phenanthroline molecule are observed in the range of 1560 cm^{-1} in the spectrum, and the band around 736 cm^{-1} in the spectrum arises due to the valence vibrations of the C-H bonds in the 1,10-phenanthroline molecule.

The FT-IR spectrum of the synthesized complex is shown in Figure 7. Compared to the spectrum of the ligand 1,10-phenanthroline (Figure 6), the stretching vibration peaks of the C=N (υ C=N, 1616 cm-1) and C=C (υ C=C, 1587 cm^{-1}) in the 1,10-phenanthroline ligand shifted to 1608 and 1579 cm^{-1}, respectively. The absorption bands corresponding to the vibrations occurring in the ring plane of the 1,10-phenanthroline molecule shifted in the spectrum from 1560 cm^{-1} to the range of 1519 cm^{-1}, and the valence vibration bands of the C-H bonds shifted from 736 cm^{-1} in the ligand to 719 cm^{-1} in the complex. The stretching vibration absorption bands of the C=C double bond shifted to blue, while the other absorption bands shifted to red, indicating that the nitrogen atoms of the heterocyclic ligand 1,10-phenanthroline are coordinated with the Cu^{2+} ion. Additionally, the vibrational bands at 621 cm^{-1} in the complex indicate the presence of the Cu-N bond [16-19].

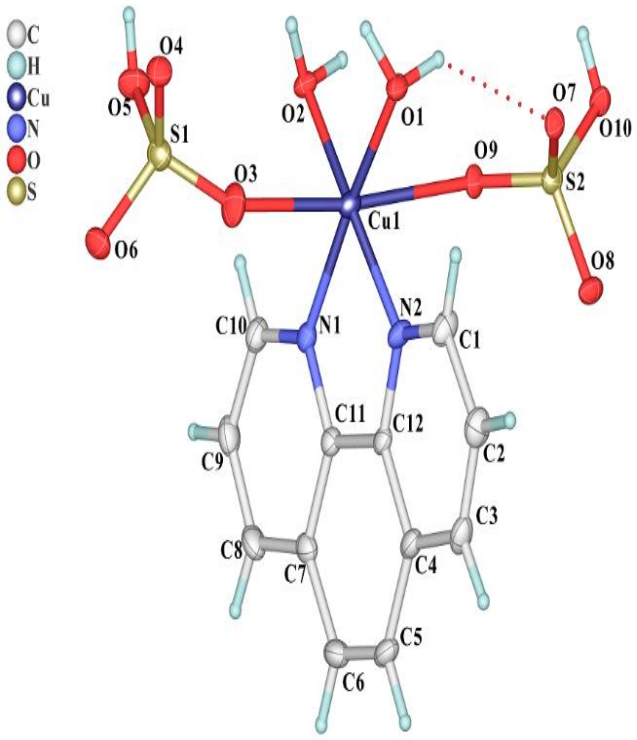

Fig. 3 View of the molecular structure of complex

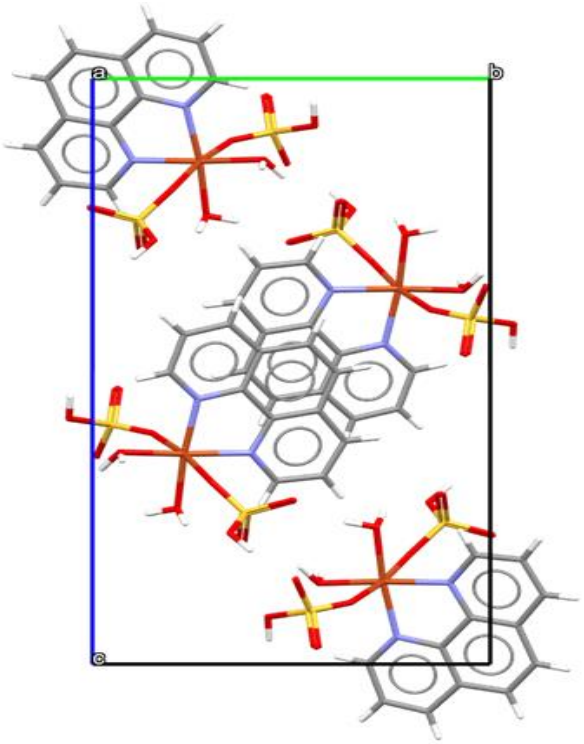

Fig. 4 Packing diagram of the complex seen along the crystallographic axis

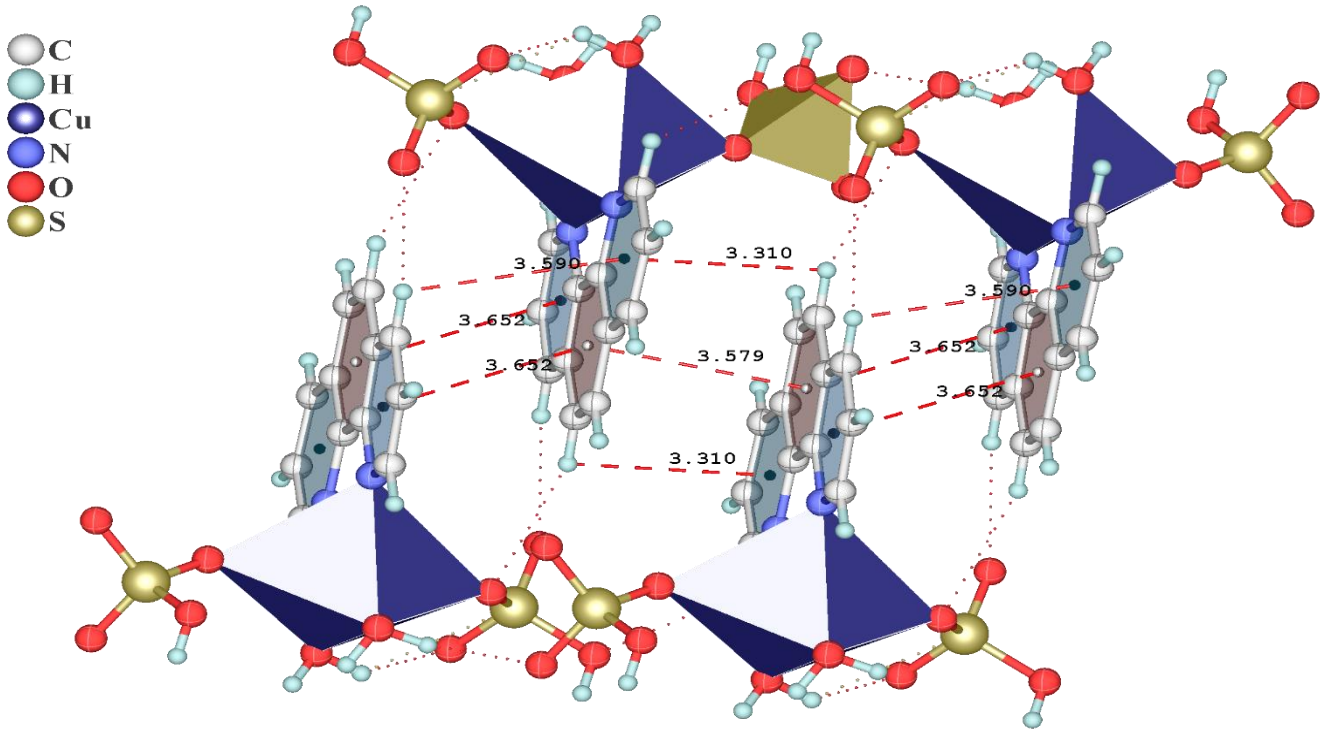

Fig. 5 The crystal packing of the complex is shown by H-bonding and p-p interactions. For clarity, only hydrogen bonding atoms and π-π interaction atoms are given

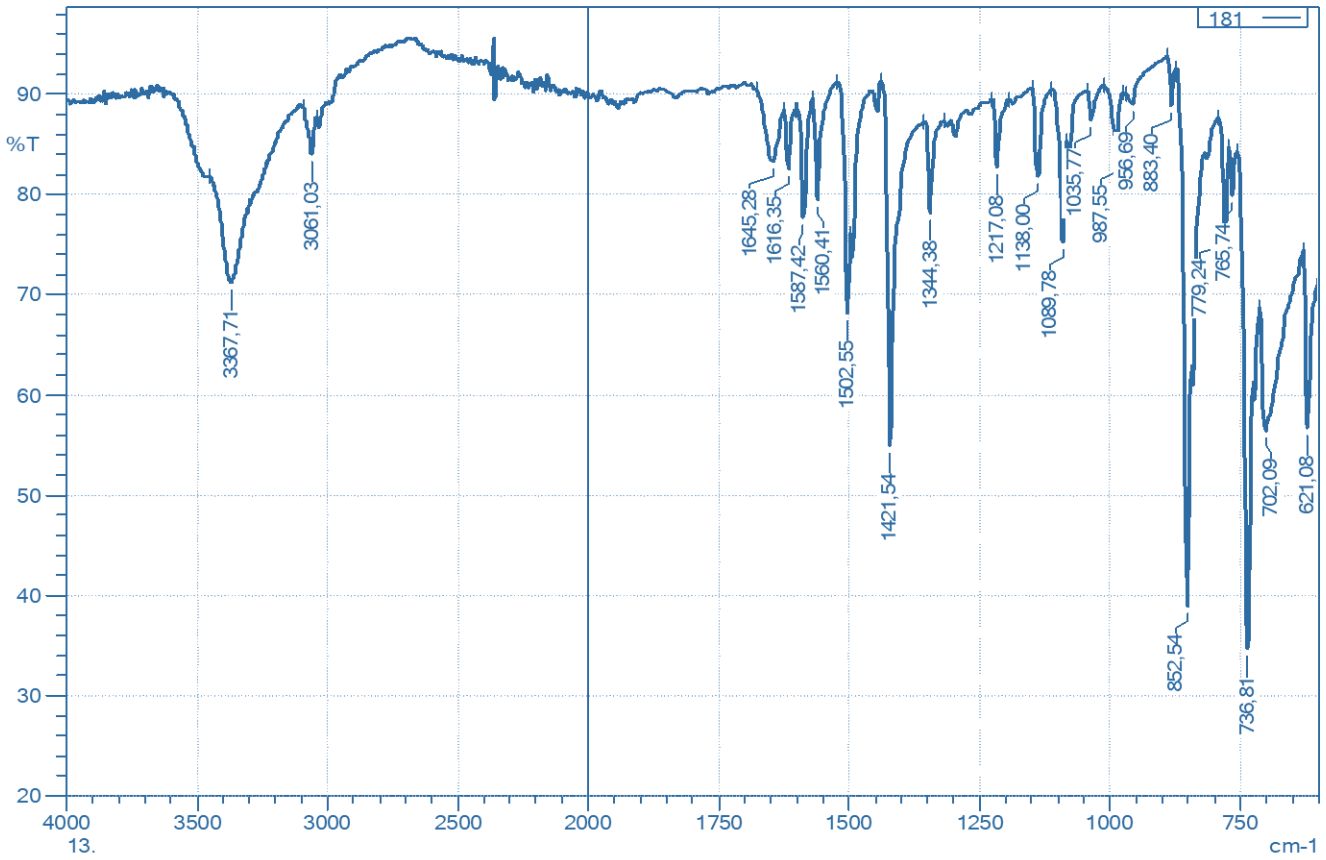

Fig. 6 IR spectrum analysis of ligand

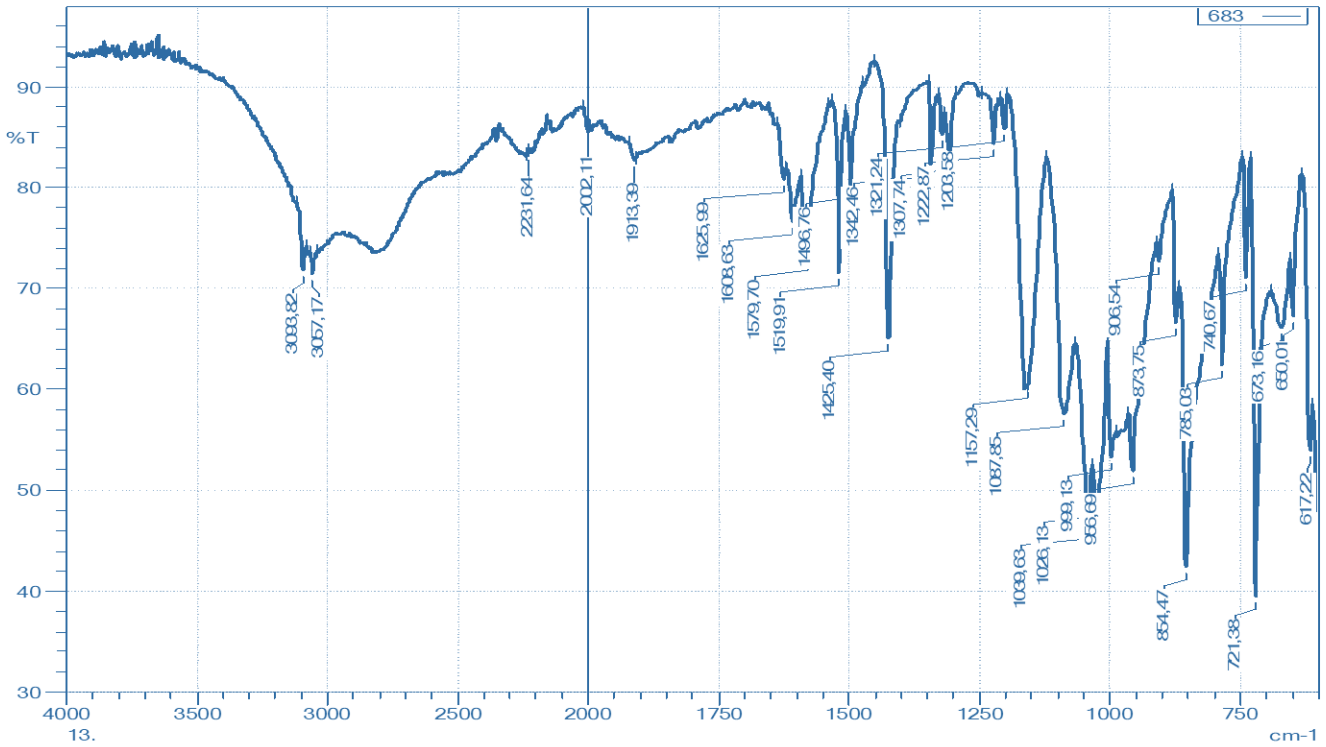

Fig. 7 IR-spectrum analysis of the complex compound

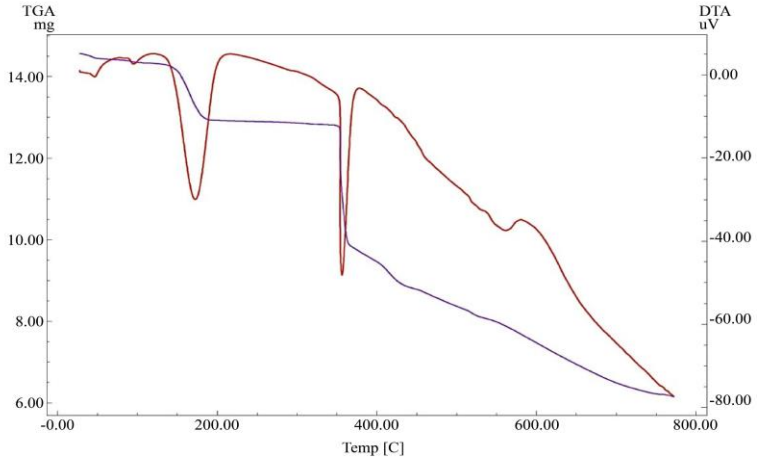

Fig. 8 Derivatogram of the complex sample. TGA - Thermogravimetric analysis curve; DTA - Differential thermal analysis curve

3.3. Thermal Analysis of Copper (II) Complexes

The derivatogram of the complex sample, which consists of two curves, is shown in Figure 8. On the Derivatogram (DTA) curve, three endothermic effects were detected at 95.010°C, 172.260°C, 356.150°C, and 561.36°C, and no exothermic effect was observed. Analysis of the Thermogravimetric Analysis (TGA) curve indicates that the TGA curve undergoes four intensive decomposition temperature ranges. The first endothermic effect occurs around 41.84-145.800°C, with a mass loss of 0.293 mg (100-200°C), which is explained by the loss of residual water used as a solvent. The second endothermic effect occurs around 144.80-348.110°C, with a mass loss of 1.412 mg. The third endothermic effect is observed in the range of 350.57-434.160°C, with a mass loss of 3.908 mg, which is explained by the decomposition of the sulfate anion in the complex. The fourth endothermic effect is observed in the range of 434.16-768.170°C, with a mass loss of 2.713 mg, which is explained by the breaking and decomposition of the sulfate anion and 1,10-phenanthroline bonds. The total mass loss in the temperature interval of 41.84-609.42.75 °C was found to be 8.326 mg, taking 76.66 minutes. The analysis of the thermogravimetric analysis curve and the differential thermal analysis curve is presented in Table 3. From the table, it can be seen that the highest mass loss occurs in the third decomposition interval, where 26.83% of the mass is lost.

Table 3. Analysis of the Thermogravimetric Analysis (TGA) curve

Temperature ^{0}C	Time, minute	Weight (mg)	Lost Weight (%)
41,84-145,80	10,68	0,293	2,01
144,80-348,11	20,54	1,412	9,69
350,57-434,16	8,51	3,908	26,83
434,16-768,17	34,67	2,713	18,63

The detailed analysis of the thermogravimetric analysis curve and the differential thermal analysis curve is presented in Table 4.

Table 4. Effect of temperature on weight loss of complex sample

No	Dw 14,56	1/T	dw/dt	M.g	Mint	T^0+K
1	14,37	0.0026	0,026	0,18	7,15	373
2	12,94	0.0021	0,094	1,61	17,16	473
3	12,87	0.0017	0,062	1,69	27,16	573
4	9,60	0.0014	0,133	4,95	37,16	673
5	8,49	0.0012	0,128	6,06	47,16	773
6	7,67	0,0011	0,121	6,88	57,13	873
7	6,68	0,0010	0,117	7,87	67,10	973
8	6,15	0,0009	0,109	8,40	77,05	1073

The activation energy values of this process for the complex are shown in Table 5.

Table 5. Results of the Thermal-oxidation analysis of the complex

No	Dw 14,56	Ln(W_1/W_2)	1/T *10^{-3}
1	14,37	0,0130	2.6
2	12,94	0,1176	2.1
3	12,87	0,1234	1.7
4	9,60	0,4161	1.4
5	8,49	0,5390	1.2
6	7,67	0,6408	1.1
7	6,68	0,7789	1.0
8	6,15	0,8614	0.9

Thus, based on the experimental data obtained on the kinetics of the processes in the temperature range from 41.84 to 1073 K, the characteristics of the thermal-oxidative degradation of the complex sample were studied.

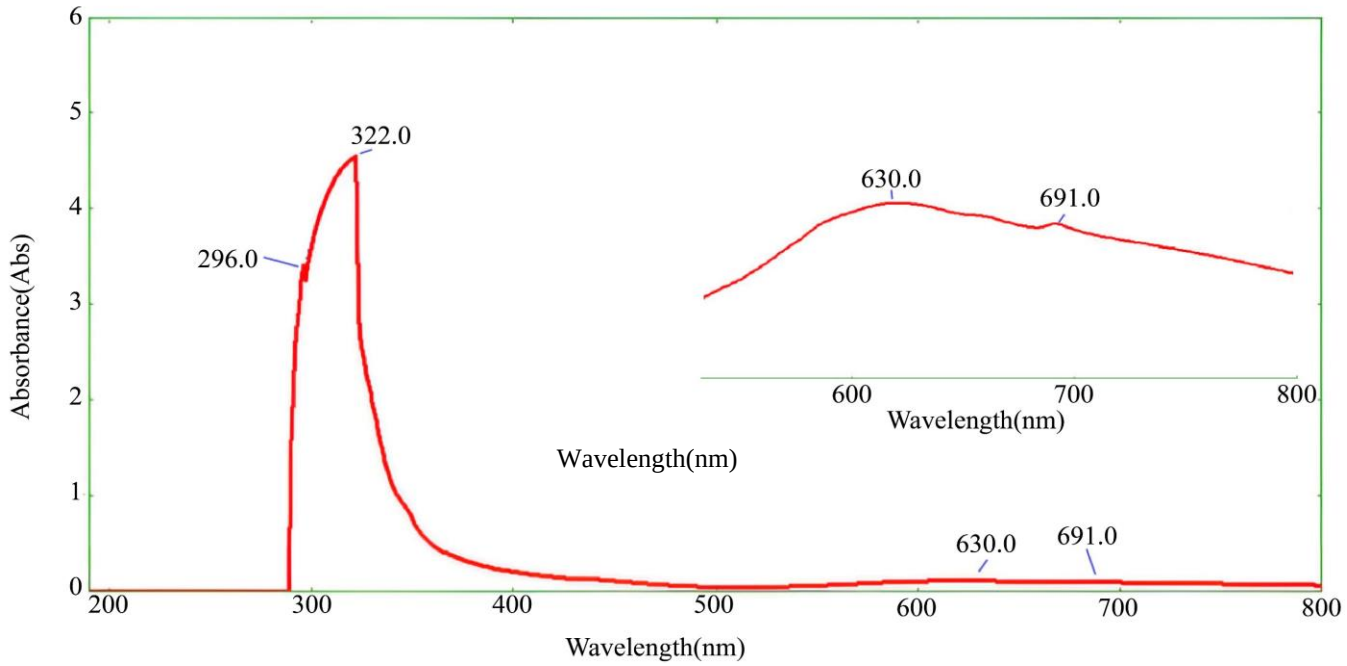

Fig. 9 UV-vis spectrum analysis of the complex compound

3.4. UV–vis Spectrum Copper (II) Complexes

The complex was dissolved in DMF to prepare a 0.05 molar solution, and its UV spectrum was recorded using a UV-vis spectrophotometer EMC-30PC-UV [16] (Figure 9). Shifts in the maximum absorption wavelengths corresponding to π→π* (C=C), π→π* (C=N), and n→π* (C=N) transitions in the ligand were observed upon coordination of the ligand to the metal. In the complex, absorptions occurred at 296 nm, 322.0 nm, 630 nm, and 691 nm, corresponding to π→π* (C=N), π→π* (C=N), n→π* (C=N), and Cu→O transitions, respectively. Compared to the salt, the increase in absorption wavelength can be related to the formation of stronger and shorter equatorial Cu-N bonds with a strong field phenanthroline, leading to an increase in the length of the axial Cu-OSO3H bond. Consequently, the energy gap between the dz2 and dxy orbitals decreases, reducing the gap between the 2B2g and 2A1g energy states.

3.5. Hirshfeld Surface Analysis

To understand the presence of molecular interactions and to determine the stability of the crystal lattice, we conducted a Hirshfeld surface analysis using Crystal Explorer 21.5. The $SO_4H\cdots O$ hydrogen bond was identified as one of the important structure-forming interactions in crystal packing [20, 21]. Hirshfeld surface analysis provides information about the quantitative ratio of short contacts and also indicates their locations. Various maps of the Hirshfeld surface are shown in Figure 10. The red and blue triangles on the shape-index map (Figure 10b) indicate the presence of π–π interactions in the complex molecule. The complex molecule is arranged in planar stacking. Bright red spots in the Hirshfeld surface analysis indicate strong intermolecular H-bond interactions ($SO_4H\cdots O$), while smaller light red spots indicate CH···O interactions (Figure 11). The Hirshfeld analysis also indicates relatively weak interactions present in the crystal lattice. The Hirshfeld fingerprint diagrams, obtained using the de and di functions, which indicate the sensitivity of individual molecular interactions to the crystal packing, are shown in the graphs of the 2D fingerprint plots. As a result of the analysis of the Hirshfeld surface, the following interactions were identified: H···O/O···H, H···H, H···C/C···H, C…C, O…O, H···N/N···H, O…C/C…O, and N…C/C…N contacts, represented by 2D fingerprint plots in Figure 12. The most significant intermolecular interactions are H···O/O···H, which plays a crucial role in the overall crystal packing, contributing to 56.2%, and is located in the inner and middle regions of the fingerprint area. H···H interactions are located in the middle region of the fingerprint area, contributing 19.2%. H···C/C···H interactions are located in the middle and side parts of the fingerprint area, contributing 11.5%. C…C interactions are located at the center of the fingerprint area, contributing 7.2%. Weak O…O, H···N/N···H, O…C/C…O, and N…C/C…N interactions account for 2.8%, 1.6%, 1.4%, and 0.2% of the fingerprint area, respectively.

In CrystalExplorer software, it is possible to visualize the "void" regions of the crystal structure of the complex. In CrystalExplorer 21.5, the void surface was identified as an isosurface of the procrystal electron density and calculated for the unit cell. The standard value is 0.002 e Å^3. The void surface for the complex is shown in Figure 13. The volume of the voids in the unit cell was determined to be 146.98 Å³, with a surface area of 538.04 Å², and it accounts for 8.73% of the total volume.

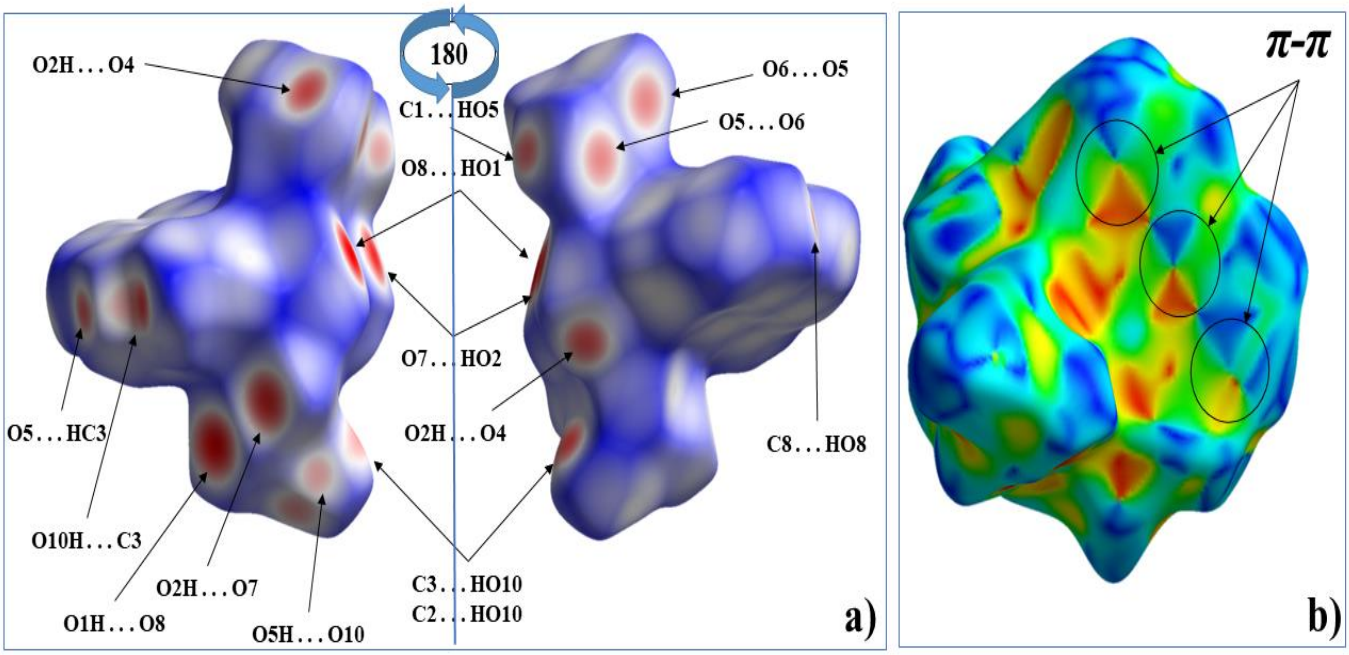

Fig. 10 Hirshfeld surfaces mapped over (a) d_{norm}, (b) Shape index

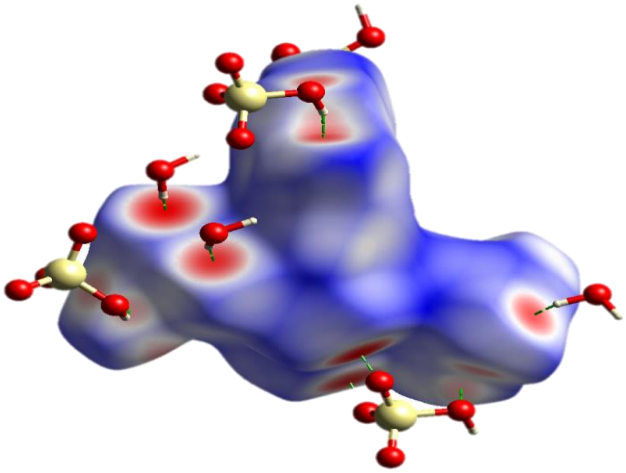

Fig. 11 Hirshfeld surface plotted based on dnorm: (SO_4H···O) bonds

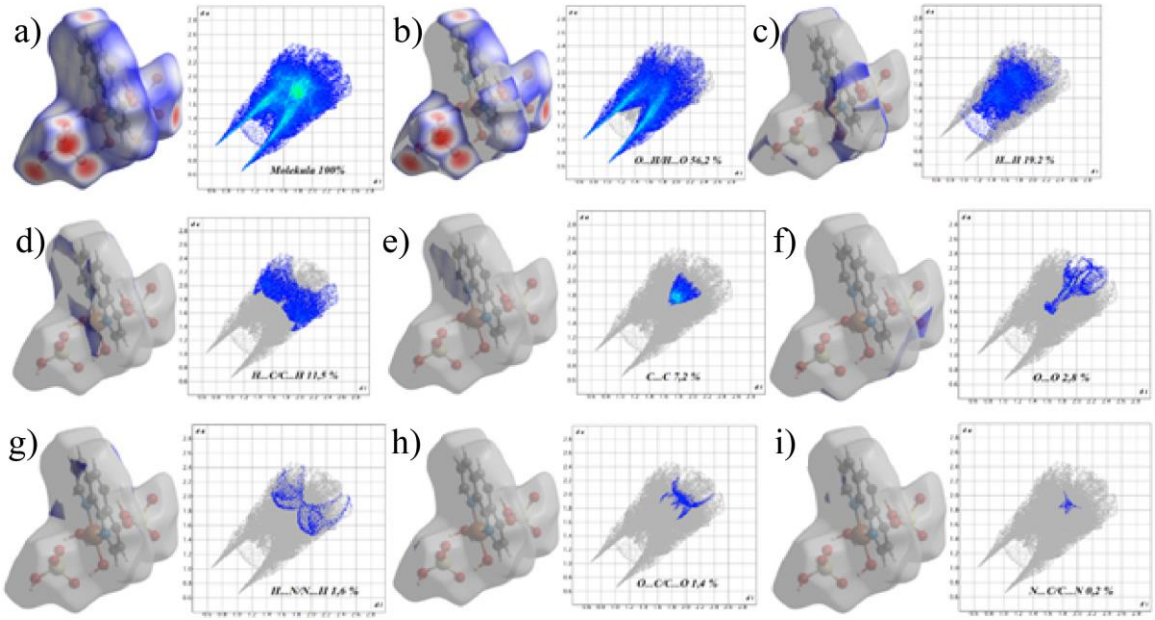

Fig. 12 a) all interactions in the crystal packing and b) H···O/O···H, c) H···H, d) H···C/C···H, e) C…C, f) O…O, g) H··· 2D fingerprint plots depicting individual N/N···H, h) O…C/C…O, and i) N…C/C…N interactions

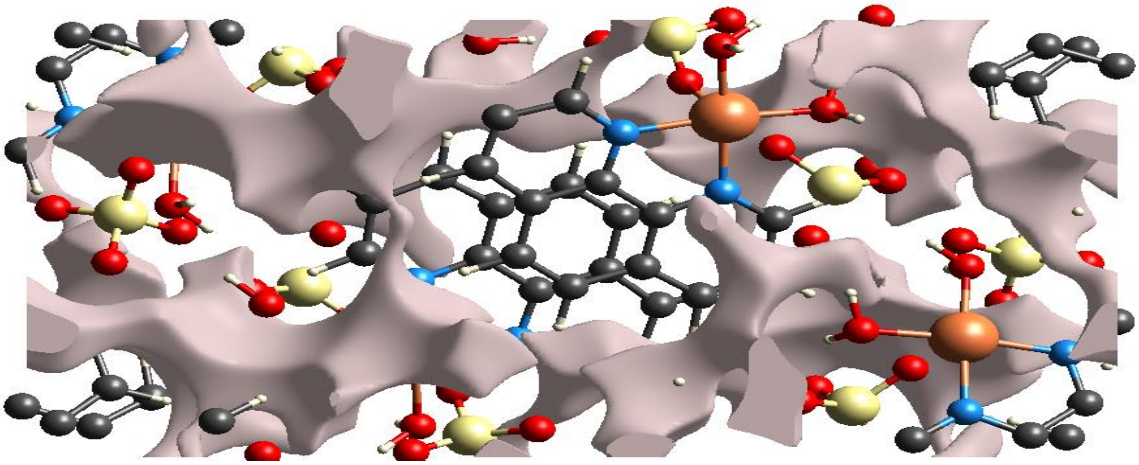

Fig. 13 Graphical representation of the voids in the crystal lattice along the a-axis

4. Conclusion

It is possible to say this concisely: optimal conditions for the formation of complexes of Cu (II) with 1,10-phenanthroline have been investigated. The obtained complexes were separated, and their structure and other properties were analyzed by various physicochemical methods (X-ray diffraction analysis, Elemental analysis, IR spectrum, DTA, TGA, UV-vis, and Hirshfeld Surface analysis). Based on the results of the analysis, the exact structural formula of the obtained complex was proposed, and a CCDC Deposit number was obtained.

Acknowledgment

Authors thank Termez State University and the Institute of Bioorganic Chemistry, named after O.S.Sodikov AS RUz, for supporting this research work.

References

[1] Qian Chu et al., "Syntheses, Structures, And Optical Properties of Novel Zinc (II) Complexes with Multicarboxylate and N-Donor Ligands," *Dalton Transactions*, no. 38, pp. 4302-4311, 2007. [CrossRef] [Google Scholar] [Publisher Link]

[2] Kathryn E. Erkkila, Duncan T. Odom, and Jacqueline K. Barton, "Recognition and Reaction of Metallointercalators with DNA," *Chemical Reviews*, vol. 99, no. 9, pp. 2777-2796, 1999. [CrossRef] [Google Scholar] [Publisher Link]

[3] Haim Tapiero, D.M. Townsend, and Kenneth D. Tew, "Trace Elements in Human Physiology and Pathology. Copper," *Biomedicine & Pharmacotherapy*, vol. 57, no. 9, pp. 386-398, 2003. [CrossRef] [Google Scholar] [Publisher Link]

[4] Geoffrey Wilkinson, Gillard R.D, and McCleverty J. A., "Comprehensive Coordination Chemistry. The Synthesis, Reactions, Properties and Applications of Coordination Compounds. V. 3. Main Group and Early Transition Elements," *Main group and early transition elements*, 1987. [Google Scholar] [Publisher Link]

[5] Nora M. Urquiza et al., "Inhibition Behavior on Alkaline Phosphatase Activity, Antibacterial and Antioxidant Activities of Ternary Methimazole-Phenanthroline-Copper (II) Complex," *Inorganica Chimica Acta*, vol. 405, pp. 243-251, 2013. [CrossRef] [Google Scholar] [Publisher Link]

[6] Livia Viganor et al., "The Antibacterial Activity of Metal Complexes Containing 1, 10-Phenanthroline: Potential as Alternative Therapeutics in The Era of Antibiotic Resistance," *Current Topics in Medicinal Chemistry*, vol. 17, no. 11, pp. 1280-1302, 2017. [CrossRef] [Google Scholar] [Publisher Link]

[7] Abror Nomozov et al., "Synthesis of Corrosion Inhibitors Based on (Thio)Urea, Orthophosphoric Acid and Formaldehyde and Their Inhibition Efficiency," *Baghdad Science Journal*, vol. 22, no. 4, 2024. [CrossRef] [Google Scholar] [Publisher Link]

[8] Chang-Feng Wang et al., "A Novel Co-Crystallization Molecular Ferroelectric Induced by The Ordering of Sulphate Anions and Hydrogen Atoms," *Inorganic Chemistry Frontiers*, vol. 5, no. 10, pp. 2413-2419, 2018. [CrossRef] [Google Scholar] [Publisher Link]

[9] Sujittra Youngme et al., "Structural Diversities and Spectroscopic Properties of Bis and Tris (1, 10-Phenanthroline) Copper (Ii) Complexes," *Polyhedron*, vol. 26, no. 7, pp. 1459-1468, 2007. [CrossRef] [Google Scholar] [Publisher Link]

[10] Xin Hu et al., "Two New Supermolecular Structures of Organic-Inorganic Hybrid Compounds: $[Zn(phen)(SO_4)(H_2O)_2]_n$ and $[Cu(phen)(H_2O)_2]\cdot SO^4$ (phen= 1, 10-phenanthroline)," *Inorganica Chimica Acta*, vol. 362, no. 10, pp. 3421-3426, 2009. [CrossRef] [Google Scholar] [Publisher Link]

[11] Mokhichekhra Shaymardanova et al., "Studying of The Process of Obtaining Monocalcium Phosphate based on Extraction Phosphoric Acid from Phosphorites of Central Kyzylkum," *Baghdad Science Journal*, vol. 22, no. 1, 2024. [CrossRef] [Google Scholar] [Publisher Link]

[12] M.A. Shaymardanova et al., "Study of Processe of Obtaining Monopotassium Phosphate Based on Monosodium Phosphate and Potassium Chloride," *Chemical Problems*, no. 3, pp. 279-293, 2023. [CrossRef] [Google Scholar] [Publisher Link]

[13] Nomozov Abror Karim ugli et al., Salsola Oppositifolia Acid Extract as a Green Corrosion Inhibitor for Carbon Steel," *Indian Journal of Chemical Technology*, vol. 30, no. 6, pp. 872-877, 2023. [CrossRef] [Google Scholar] [Publisher Link]

[14] Abror Nomozov, "A Studying Synthesis of a Chelate-Forming Sorbent Based on Urea-Formaldehyde and Diphenylcarbazone," *Indian Journal of Chemistry*, vol. 63, no. 6, pp. 579-585, 2024. [CrossRef] [Google Scholar] [Publisher Link]

[15] Clare F. Macraea et al., "Mercury 4.0: From Visualization to Analysis, Design and Prediction," *Journal of Applied Crystallography*, vol. 53, no. 1, pp. 226-235, 2020. [CrossRef] [Google Scholar] [Publisher Link]

[16] Peter R. Spackmana et al., "Crystalexplorer: A Program for Hirshfeld Surface Analysis, Visualization and Quantitative Analysis of Molecular Crystals," *Journal of Applied Crystallography*, vol. 54, no. 3, pp. 1006-1011, 2021. [CrossRef] [Google Scholar] [Publisher Link]

[17] P. Dhamodharan, K. Sathya, and M. Dhandapani, "Systematic Evaluation of A New Organic Material: 1-Methyl-1h-Imidazol-3-Ium-2,4,6-Trinitrobenzene-1,3-Bis(Olate) for Optoelectronics Through Spectral, Structural, Electrical, Optical, Quantum Chemical and Hirshfeld Surface Studies," *Journal of Physics and Chemistry of Solids*, vol. 104, pp. 175-184, 2017. [CrossRef] [Google Scholar] [Publisher Link]

[18] Mark A. Spackman, and Dylan Jayatilaka, "Hirshfeld Surface Analysis," *CrystEngComm*, vol. 11, no. 1, pp. 19-32, 2008. [CrossRef] [Google Scholar] [Publisher Link]

[19] Abror Nomozov, “Spectrophotometric Determination of Copper(II) Ion with 7-Bromo-2-Nitroso-1-Oxinaphthalene-3,6-Disulphocid,” *Indian Journal of Chemistry*, vol. 63, no. 5, pp. 500-505, 2024. [CrossRef] [Google Scholar] [Publisher Link]

[20] Gulnora A. Umirova et al., “Crystal Structure and Hirshfeld Surface Analysis of 8-Aza-Niumylquinolinium Tetra-Chlorido-Zincate(II), ”*Crystallographic Communications*, vol. 79, no. 9, pp. 856-861, 2023. [CrossRef] [Google Scholar] [Publisher Link]

[21] F.S. Narmanova et al., “The Structure and Hirshfeld Surface Analysis of the 4-Amino 3-Nitrobenzoic Acid Triclinic Polymorph,” *Structural Chemistry*, vol. 35, pp. 953-960, 2024. [CrossRef] [Google Scholar] [Publisher Link]